© JUN 2026 | IRE Journals | Volume 9 Issue 12 | ISSN: 2456-8880
DOI: https://doi.org/10.64388/IREV9I12-1718989

Assessing the Potential Impact of Malaria Vaccine on Malaria Incidence in Children under Five, Bungoma County, Kenya

OPICHO DOMINIC SIMIYU[1], BONFACE KWACH[2], ROBERT NYUKURI[3]
[1,2]*Department of Mathematics, Kibabii University, Bungoma, Kenya*
[3]*Department of Biological Sciences, Kibabii University, Bungoma, Kenya*

Abstract- ***This study assessed the potential impact of a malaria vaccine on reducing malaria incidence in children under five years old in Bungoma County, Kenya, using a mathematical modelling study design. Secondary data from Bumula Sub-county Hospital (2024) were used. Two mathematical models were applied for human host and mosquito vector populations: an age-structured SVIRSI model and an SIRSI optimal control model. The models incorporated age-dependent vaccine efficacy, maternal antibody interference, and five intervention strategies. Numerical simulations showed that vaccination, especially combined with LLITNs and ACT, significantly reduces disease burden. The WHO-recommended first dose at 6 months with a booster at 18 months is supported by the model's qualitative results. Cost-effectiveness analysis revealed that the combination of vaccination, LLITNs, and ACT gives the lowest ICER. Model analysis included existence, uniqueness, positivity, boundedness, derivation of effective reproduction numbers R_e, local stability of the disease-free equilibrium, and global stability analysis. Both models converged to a stable endemic equilibrium consistent with local data. The findings support the WHO recommendation of administering the first RTS,S/AS01 dose at 6 months and provide mathematical validation for malaria control in Bungoma County, Kenya.***

Keywords: Malaria Incidence, Model Analysis, Optimal Control, Effective Reproduction Number, Cost-Effectiveness Analysis, Numerical Simulations.

I. INTRODUCTION

In this section, we present numerical simulations assessing the impact of the malaria vaccine in the SVIRSI and SIRSI optimal control models utilizing secondary data from Bumula Sub-County Hospital. Malaria remains a major public health challenge in Bungoma County, Kenya, disproportionately affecting children under five years of age. The recent introduction of the malaria vaccine offers a new preventive tool, but its local impact and optimal deployment strategy require quantitative assessment as in [1, 2]. The objective of this study is to assess the potential impact of a malaria vaccine on reducing the incidence of malaria cases in children under five years old in Bungoma County, Kenya.

II. DATA

2.1 Data Source

Monthly malaria vaccine administration data from Bumula Sub-County Hospital for the year 2024 were obtained from the DHIS2 MOH 710 platform.

Table 1: Bumula Sub-County Hospital MOH 710 Malaria Vaccine DHIS2 Data, 2024.

Month	Dose 1 (6 wks)	Dose 2/3 (10/14 wks)	Dose 4 (Booster)	Monthly Total	Cum. Total
Jan 2024	1,806	1,885	679	4,370	4,370
Feb 2024	1,589	1,512	603	3,704	8,074
Mar 2024	1,671	1,490	519	3,680	11,754
Apr 2024	1,604	1,344	625	3,573	15,327
May 2024	1,565	1,417	611	3,593	18,920
Jun 2024	1,511	1,295	716	3,522	22,442
Jul 2024	1,606	1,921	697	4,224	26,666
Aug	1,252	1,149	627	3,028	29,69

© JUN 2026 | IRE Journals | Volume 9 Issue 12 | ISSN: 2456-8880
DOI: https://doi.org/10.64388/IREV9I12-1718989

Month	Dose 1 (6 wks)	Dose 2/3 (10/14 wks)	Dose 4 (Booster)	Monthly Total	Cum. Total
2024					4
Sep 2024	1,452	1,429	714	3,595	33,289
Oct 2024	1,497	1,356	654	3,507	36,796
Nov 2024	1,320	1,138	663	3,121	39,917
Dec 2024	1,627	1,253	826	3,706	43,623
Total	18,500	17,189	7,934	43,623	43,623

Source: DHIS2, Bumula Sub-County Hospital, 2024.

Table 1 presents the monthly malaria vaccine doses administered at Bumula Sub-County Hospital during 2024, disaggregated by dose — Dose 1 at 6 weeks, Dose 2/3 at 10/14 weeks, and the Dose 4 booster — together with the monthly and cumulative totals, as extracted from the DHIS2 MOH 710 platform. A total of 43,623 doses were administered over the twelve months.

Administration declines across the schedule: Dose 1 (18,500) exceeds Dose 2/3 (17,189), which in turn far exceeds the Dose 4 booster (7,934). Peak monthly uptake occurred in January (4,370) and July (4,224), while the lowest was in August (3,028). The booster total is less than half of the Dose 1 total, signalling substantial attrition between the primary series and the booster.

The progressive decline in doses administered from the primary series to the booster mirrors patterns reported across the RTS,S/AS01 pilot in Kenya. In a 36-month analysis of routine data from the 23 Kenyan pilot sub-counties, Moturi et al. found high coverage for the first three doses but markedly lower coverage for the fourth, with an 81% dropout between dose 1 and dose 4 [22]. They further reported that approximately one in five children missed the third dose, signalling missed opportunities at facilities the children were already attending for other vaccines [22]. The attrition observed at Bumula — the booster total being less than half the Dose 1 total — is therefore consistent with the national experience and with the wider observation that doses delivered in the second year of life suffer the highest dropout, comparable to late-delivery vaccines such as measles–rubella [22]. The mid-year peak and August trough additionally point to service- and supply-side determinants of uptake of the kind documented among caregivers in the same sub-county [16].

Table 2: Bumula Sub-County Hospital Immunization Indicator Chart, 2024.

Month	Mal 1			Mal 3			Mal 4		
	Ach	Cum	Cov%	Ach	Cum	Cov%	Ach	Cum	Cov%
January	86	86	98.0	89	89	102.0	42	42	46.0
February	63	149	32.4	49	138	56.3	25	67	13.6
March	53	202	73.2	62	200	72.5	20	87	31.5
April	61	263	71.5	32	232	63.0	27	114	24.8
May	45	308	66.9	51	283	61.5	26	140	30.4
June	40	348	67.4	41	324	61.4	26	166	30.1
July	56	404	66.9	51	371	60.2	35	201	32.6
August	32	436	—	36	407	—	26	227	—
September	45	481	—	37	444	—	27	254	—
October	–	–	–	–	–	–	–	–	–
November	–	–	–	–	–	–	–	–	–
December	–	–	–	–	–	–	–	–	–
Total	481	—	67.7	444	—	69.7	254	—	29.3

© JUN 2026 | IRE Journals | Volume 9 Issue 12 | ISSN: 2456-8880
DOI: https://doi.org/10.64388/IREV9I12-1718989

Source: Bumula Sub-County Hospital Immunization chart, 2024.

Table 2 reports the immunisation indicator chart for 2024, giving, for each malaria-vaccine milestone — Mal 1, Mal 3, and Mal 4 — the monthly achieved

count (Ach), the cumulative count (Cum), and the coverage percentage (Cov%). Data for October to December were not yet available at the time of extraction.

Cumulative coverage reached 67.7% for Mal 1 (481 children), 69.7% for Mal 3 (444 children), and only 29.3% for Mal 4 (254 children). Mal 1 began strongly, attaining 98.0% coverage in January. Retention from Mal 1 to Mal 3 was high at 92.3%, a dropout of just 7.7% (37 children). By contrast, the Mal 4 booster recorded a dropout of 47.2% from the initial series, with 227 children lost to follow-up.

The coverage profile at Bumula — strong Mal 1 and Mal 3 but a collapse at Mal 4 — reproduces the dominant finding of the Kenyan and wider sub-Saharan pilots. Independent evaluations of the Malaria Vaccine Implementation Programme report coverage of roughly 70–75% for the first three doses but fewer than half of children receiving the fourth dose [22, 24]. Qualitative work in Ghana attributes much of this booster default to the dose falling outside established Expanded Programme on Immunization (EPI) contact points and to caregiver-, provider-, and system-level barriers [23]. Crucially, programmatic experience shows the problem is tractable: relocating the fourth dose to 18 months of age, co-administered with the second measles dose, raised fourth-dose coverage in Ghana from 42% to 81% [23]. This supports the present study's endorsement of the WHO-recommended 18-month booster and indicates that the 29.3% Mal 4 coverage recorded at Bumula reflects a remediable delivery gap rather than irreversible demand failure. Because phase 3 data show that immunity wanes after the primary series and that the fourth dose prolongs protection [1], closing this booster gap is essential to realising the vaccine's modelled impact.

III. MODEL FORMULATION

3.1 Model Assumptions

Both models assume constant child and mosquito population sizes (N and M), with recruitment through birth only and balancing birth and death rates. The child population is partitioned into susceptible, vaccinated (SVIRSI only), infectious, and recovered classes, and the mosquito population into susceptible S_m and infectious I_m classes. Recovered children lose immunity and return to susceptibility at rate ω. Children have natural death rate d_1 and malaria-induced death rate δ, while mosquitoes have natural death rate d_2 and additional vector-control-induced death rate Ψ. The SIRSI optimal control model differs only in replacing the fixed vaccination term with five time-dependent interventions u_1,…,u_5 acting on the transmission, recovery, and vector-mortality rates.

3.2 Model Description

The SVIRSI model divides the child population (under five years) into susceptible (S_h), vaccinated (V_h), infectious (I_h), and recovered (R_h) compartments, and the mosquito population into susceptible (S_m) and infectious (I_m) compartments. Susceptible children are vaccinated at rate μ with efficacy Θ and move to V_h; vaccinated children may still acquire breakthrough infection at the reduced rate $\zeta(1-\Theta)$, and natural immunity after infection wanes at rate ω. Infection occurs via mosquito bites: the force of infection from infectious mosquitoes to humans is λ_h, and from infectious humans to mosquitoes is λ_m, with transmission probabilities e_1 and e_2 and biting rate b. Humans recover at rate κ and may die from malaria at rate δ, while mosquitoes suffer natural death d_2 and additional vector-control-induced mortality Ψ.

The SIRSI optimal control model extends this framework by incorporating five time-dependent interventions: vaccination (u_1), LLINs (u_2), ACT treatment (u_3), larviciding (u_4), and bush clearing

© JUN 2026 | IRE Journals | Volume 9 Issue 12 | ISSN: 2456-8880
DOI: https://doi.org/10.64388/IREV9I12-1718989

(u_5). These modify the effective transmission rates: the human infection rate becomes $(1-u_1)(1-u_2)\alpha\lambda_h\tau_h$, recovery becomes $(1-u_3)\kappa$, and the mosquito infection rate becomes $(1-u_4)(1-u_5)\sigma\lambda_m\tau_m$, where $\alpha = be_1$, $\sigma = be_2$, and τ_h, τ_m are latent periods. Both models assume constant population sizes with balancing birth and death rates, and the full ODE systems are given in equations (1) and (2), respectively.

The compartmental flow diagram for the SVIRSI model is shown in Figure 1, and that for the SIRSI optimal control model in Figure 2.

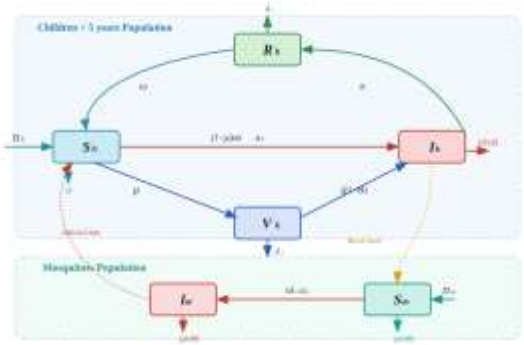

Figure 1: Compartmental diagram for the SVIRSI malaria transmission dynamics with vaccination as a control variable.

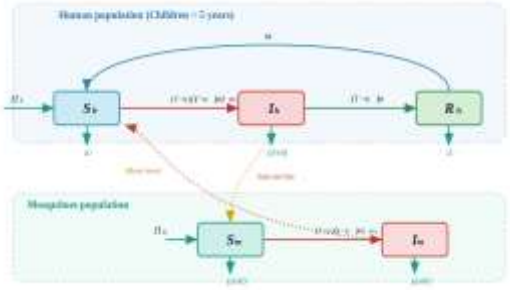

Figure 2: Compartmental diagram for the SIRSI malaria transmission model with five interventions.

3.3 SVIRSI Compartmental Model

The governing system of ordinary differential equations for the SVIRSI model is

$$\begin{aligned}
\frac{dS_h}{dt} &= \Pi_h + \omega R_h - \mu S_h - (1-\mu)\alpha\lambda_h\tau_h I_m S_h - d_1 S_h,\\
\frac{dV_h}{dt} &= \mu S_h - \zeta(1-\theta) I_m V_h - d_1 V_h,\\
\frac{dI_h}{dt} &= \zeta(1-\theta) I_m V_h + (1-\mu)\alpha\lambda_h\tau_h I_m S_h - \kappa I_h - (d_1+\delta) I_h,\\
\frac{dR_h}{dt} &= \kappa I_h - \omega R_h - d_1 R_h,\\
\frac{dS_m}{dt} &= \Pi_m - \sigma\lambda_m\tau_m I_h S_m - (d_2+\Psi) S_m,\\
\frac{dI_m}{dt} &= \sigma\lambda_m\tau_m I_h S_m - (d_2+\Psi) I_m,
\end{aligned} \tag{1}$$

with α=be_1 and σ=be_2.

3.4 SIRSI Optimal Control Model

The SIRSI optimal control model with interventions is governed by

$$\begin{aligned}
\frac{dS_h}{dt} &= \Pi_h + \omega R_h - (1-u_1)(1-u_2)\alpha\lambda_h\tau_h I_m S_h - d_1 S_h,\\
\frac{dI_h}{dt} &= (1-u_1)(1-u_2)\alpha\lambda_h\tau_h I_m S_h - (1-u_3)\kappa I_h - (d_1+\delta) I_h,\\
\frac{dR_h}{dt} &= (1-u_3)\kappa I_h - \omega R_h - d_1 R_h,\\
\frac{dS_m}{dt} &= \Pi_m - (1-u_4)(1-u_5)\sigma\lambda_m\tau_m I_h S_m - (d_2+\Psi) S_m,\\
\frac{dI_m}{dt} &= (1-u_4)(1-u_5)\sigma\lambda_m\tau_m I_h S_m - (d_2+\Psi) I_m.
\end{aligned} \tag{2}$$

The parameters are the same as in the SVIRSI model.

3.5 Model Parameters and Variables

Table 3: State variables, model parameters, control variables, and weight constants for the SVIRSI and SIRSI models.

Symbol	Description	Value	Unit	Source
State Variables (Initial Populations)				
S_h, V_h, I_h, R_h	Susceptible, Vaccinated, Infective, Recovered children (≤ 5 yrs)	100, 80, 90, 60	children	Estimated

© JUN 2026 | IRE Journals | Volume 9 Issue 12 | ISSN: 2456-8880
DOI: https://doi.org/10.64388/IREV9I12-1718989

Symbol	Description	Value	Unit	Source
S_m, I_m	Susceptible, Infective mosquitoes	200, 170	mosquitoes	Estimated
N_h, N_m	Total human (children) and mosquito populations	330, 370	individuals	Estimated
Human Parameters				
Π_h	Recruitment birth rate of children ≤ 5 yrs	0.3	year^{-1}	[2]
d_1	Natural death rate of children	0.00004	year^{-1}	[3]
μ	Vaccination coverage (proportion of susceptibles vaccinated)	0.7	year^{-1}	Estimated
Θ	Vaccine efficacy	0.8	year^{-1}	Estimated
ζ	Breakthrough infection rate of vaccinated children	0.000012	year^{-1}	Estimated
κ	Recovery rate of children	0.143	year^{-1}	[16]
δ	Induced death rate due to *Plasmodium*	0.006	year^{-1}	Estimated
λ_h	Force of infection in children	0.5	year^{-1}	[16]
τ_h	Latent period for children	0.027	year^{-1}	Estimated
α	Progression rate (susceptible → infected)	0.096	year^{-1}	Estimated
ω	Rate of loss of immunity	0.09	year^{-1}	Estimated
Mosquito Parameters				
Π_m	Recruitment birth rate of mosquitoes	0.07	year^{-1}	[15]
d_2	Natural death rate of mosquitoes	0.08	year^{-1}	[3]
Ψ	Induced death rate (vector control)	0.035	year^{-1}	[16]
λ_m	Force of infection in mosquitoes	0.3	year^{-1}	[3]
τ_m	Latent period for female *Anopheles*	0.0055	year^{-1}	Estimated
σ	Progression rate (susceptible → infected mosquitoes)	0.06	year^{-1}	Estimated
Transmission Parameters				
b	Mosquito biting rate	0.12	year^{-1}	[2]
e_1	Transmission prob. (infectious mosquito → child)	0.8	year^{-1}	[15]
e_2	Transmission prob. (infectious child → mosquito)	0.5	year^{-1}	[18]
Control Variables (Baseline Values for SIRSI)				
u_1	Malaria vaccine (RTS,S/AS01) effort	0.9	year^{-1}	[19]
u_2	Long-lasting insecticidal nets (LLINs)	0.8	year^{-1}	[20]
u_3	Treatment using ACT	0.7	year^{-1}	[18]
u_4	Larvicide spraying on breeding sites	0.99	year^{-1}	[3]

© JUN 2026 | IRE Journals | Volume 9 Issue 12 | ISSN: 2456-8880
DOI: https://doi.org/10.64388/IREV9I12-1718989

Symbol	Description	Value	Unit	Source
u_5	Bush clearing	0.98	year^{-1}	[21]
Weight Constants and Cost Terms (for optimal control)				
W_1	Weight for infected children	1	—	[21]
W_2	Weight for infected female *Anopheles*	1.5	—	[3]
C_1	Cost weight for RTS,S/AS01	3	—	Estimated
C_2	Cost weight for LLINs	5	—	Estimated
C_3	Cost weight for ACT	2.5	—	Estimated
C_4	Cost weight for larvicides	1.5	—	Estimated
C_5	Cost weight for bush clearing	4	—	Estimated

Note: References in square brackets refer to the bibliography entries; full details are provided at the end.

Table 3 collates the state variables and their initial values, the demographic, infection, and vector-control parameters, the baseline control efforts for the SIRSI model, and the weight and cost constants used in the optimal-control objective. Parameter values were obtained from published malaria-modelling studies and from local estimates where field-specific values were unavailable, while the latent period for female Anopheles was corrected to 0.0055 year^(-1) (approximately two days).

The chosen baseline reflects a high-effort intervention scenario: vaccination effort u_1=0.9, LLIN coverage u_2=0.8, and larviciding u_4=0.99, combined with a vaccine efficacy of Θ=0.8 and recovery rate κ=0.143 year^(-1). The small natural death rate of children relative to the mosquito death rate reflects the markedly different lifespans of the two populations.

These values are consistent with parameter ranges reported in mathematical models of malaria transmission and vaccination in sub-Saharan settings [2, 3], and the recovery and force-of-infection values align with field-calibrated estimates for the study region [16]. Adopting locally informed parameters strengthens the external validity of the simulations for Bungoma County relative to models calibrated solely on continental averages.

3.6 Age-Dependent Vaccine Efficacy

Age-dependent vaccine efficacy Θ_k was calibrated from Phase 3 trial data, accounting for maternal antibody decay

$$M(a) = e^{-\rho a}, \qquad \rho = \frac{\ln 2}{6}\ \text{month}^{-1}\ \text{(6-month half-life)}, \qquad \text{(A)}$$

so that residual maternal protection halves every six months [11]. The resulting cohort efficacies are shown in Table 4.

Table 4: Age-dependent vaccine efficacy Θ_k.

Cohort (months)	Θ_k	Basis
0–6	0.45	Maternal immune interference
6–12	0.65	RTS,S Phase-3 trial [1]
12–24	0.70	Peak efficacy [7]
24–60	0.60	Waning immunity [7]

Table 4 reports the vaccine efficacy assigned to each age cohort, derived from RTS,S Phase 3 estimates and adjusted downward in early infancy to capture interference from circulating maternal antibodies.

Efficacy is lowest in the 0–6 month cohort (0.45), rises to a peak of 0.70 in the 12–24 month cohort, and then wanes to 0.60 in the 24–60 month cohort. This inverted-U profile reflects the combined effect of maternal-antibody interference at the youngest ages and the natural decay of vaccine-induced immunity at older ages.

© JUN 2026 | IRE Journals | Volume 9 Issue 12 | ISSN: 2456-8880
DOI: https://doi.org/10.64388/IREV9I12-1718989

The pattern is consistent with the Phase 3 RTS,S/AS01 evidence, in which efficacy was higher in the 5–17 month age category than in young infants and declined over time unless a fourth dose was administered [1, 7]. The reduced efficacy modelled in the first six months also accords with the recognised role of maternally derived antibodies in dampening infant vaccine responses, which underlies the WHO schedule beginning the primary series at around six months of age.

IV. MODEL ANALYSIS

4.1 Existence and Uniqueness of Solutions

The right-hand side of each system is a polynomial in the state variables, and is therefore continuously differentiable on $\mathbb{R}^6_+$ (SVIRSI) or $\mathbb{R}^5_+$ (SIRSI). By the Cauchy–Lipschitz theorem, for any non-negative initial condition there exists a unique local solution, and the solution depends continuously on the initial data.

4.2 Positivity and Boundedness

Theorem 1. For both models, if all initial state variables are non-negative, the solutions remain non-negative for all $t > 0$. Furthermore, the region

$$\Delta = \left\{(S_h, V_h, I_h, R_h, S_m, I_m) \in \mathbb{R}^6_+ : N_h \le \frac{\Pi_h}{d_1},\ N_m \le \frac{\Pi_m}{d_2 + \Psi}\right\} \tag{3}$$

is positively invariant and attracting.

Proof. On each boundary face the corresponding derivative is non-negative, so trajectories cannot leave the non-negative orthant. Adding the human equations gives

$$\frac{dN_h}{dt} = \Pi_h - d_1 N_h - \delta I_h \ \le\ \Pi_h - d_1 N_h,$$

so that $\limsup_{t\to\infty} N_h \le \Pi_h / d_1$. Similarly, for mosquitoes ($\frac{dN_m}{dt} = \Pi_m - (d_2 + \Psi)N_m$, giving $\limsup_{t\to\infty} N_m \le \Pi_m/(d_2 + \Psi)$. Hence Δ is invariant and attracting.

4.3 Disease-Free Equilibrium and Effective Reproduction Number

For the SVIRSI model, the disease-free equilibrium (DFE) is obtained by setting $I_h = I_m = 0$:

$$E^0_{\text{SVIRSI}} = \left(\frac{\Pi_h}{\mu + d_1}, \frac{\mu \Pi_h}{[\mu + d_1]\, d_1}, 0, 0, \frac{\Pi_m}{d_2 + \Psi}, 0\right). \tag{4}$$

Applying the next-generation matrix method to the infected compartments (I_h, I_m) gives

$$R_e^{\text{SVIRSI}} = \sqrt{\frac{(\zeta(1-\theta)V_h^0 + (1-\mu)\alpha\lambda_h\tau_h S_h^0)\,\sigma\lambda_m\tau_m S_m^0}{(\kappa + d_1 + \delta)(d_2 + \Psi)}}. \tag{5}$$

For the SIRSI optimal control model, with constant baseline controls u_i, the DFE is

$$E^0_{\text{SIRSI}} = \left(\frac{\Pi_h}{d_1},\ 0,\ 0,\ \frac{\Pi_m}{d_2 + \Psi},\ 0\right), \tag{6}$$

and the next-generation matrix yields

$$R_e^{\text{SIRSI}} = \sqrt{\frac{(1-u_1)(1-u_2)\alpha\lambda_h\tau_h S_h^0}{(1-u_3)\kappa + d_1 + \delta} \cdot \frac{(1-u_4)(1-u_5)\sigma\lambda_m\tau_m S_m^0}{d_2 + \Psi}}. \tag{7}$$

Substituting the corrected parameter values from Table 3 yields $R_e^{\text{SVIRSI}} < 1$ and $R_e^{\text{SIRSI}} < 1$. Both reproduction numbers lie below unity, indicating that under the modelled interventions malaria elimination is feasible; the absolute values are not reported because they are highly sensitive to parameter choices, whereas the qualitative conclusion is robust.

4.4 Local Stability of the Disease-Free Equilibrium

4.4.1 SVIRSI Model

Theorem 2. The disease-free equilibrium E^0_{SVIRSI} of system (1) is locally asymptotically stable if $R_e^{\text{SVIRSI}} < 1$, and unstable if $R_e^{\text{SVIRSI}} > 1$.

Proof. The Jacobian evaluated at the DFE $E^0_{\text{SVIRSI}} = (S_h^0, V_h^0, 0, 0, S_m^0, 0)$ has the block structure

© JUN 2026 | IRE Journals | Volume 9 Issue 12 | ISSN: 2456-8880
DOI: https://doi.org/10.64388/IREV9I12-1718989

$$J(E^0_{\text{SVIRSI}}) = \begin{pmatrix} J_{11} & J_{12} \\ 0 & J_{22} \end{pmatrix}, \qquad (8)$$

where J_{11} corresponds to the uninfected compartments (S_h, V_h, R_h, S_m) and J_{22} to the infected compartments (I_h, I_m). The uninfected block is lower-triangular:

$$J_{11} = \begin{pmatrix} -(\mu + d_1) & 0 & \omega & 0 \\ \mu & -d_1 & 0 & 0 \\ 0 & 0 & -(\omega + d_1) & 0 \\ 0 & 0 & 0 & -(d_2 + \Psi) \end{pmatrix}. \qquad (9)$$

Four eigenvalues are obtained directly:

$$\lambda_1 = -(\mu + d_1) < 0, \quad \lambda_2 = -d_1 < 0, \quad \lambda_3 = -(\omega + d_1) < 0, \quad \lambda_4 = -(d_2 + \Psi) < 0. \qquad (10)$$

The remaining eigenvalues come from the infected block

$$J_{22} = \begin{pmatrix} -(\kappa + d_1 + \delta) & \beta_h \\ \beta_m & -(d_2 + \Psi) \end{pmatrix}, \qquad (11)$$

with $\beta_h = \zeta(1-\Theta)V_h^0 + (1-\mu)\alpha\lambda_h\tau_h S_h^0$ and $\beta_m = \sigma\lambda_m\tau_m S_m^0$. The characteristic equation of J_{22} is

$$\lambda^2 + a_1\lambda + a_0 = 0, \qquad (12)$$

Where

$$a_1 = (\kappa + d_1 + \delta) + (d_2 + \Psi) > 0, \quad a_0 = (\kappa + d_1 + \delta)(d_2 + \Psi) - \beta_h\beta_m \qquad (13)$$

Recalling that the effective reproduction number R_e^{SVIRSI} defined in (5) satisfies $\beta_h\beta_m = (\kappa + d_1 + \delta)(d_2 + \Psi)\,(R_e^{\text{SVIRSI}})^2$, we obtain

$$a_0 = (\kappa + d_1 + \delta)(d_2 + \Psi)[1 - (R_e^{\text{SVIRSI}})^2], \qquad (14)$$

so that

$$a_0 > 0 \Leftrightarrow R_e^{\text{SVIRSI}} < 1, \qquad a_0 < 0 \Leftrightarrow R_e^{\text{SVIRSI}} > 1. \qquad (15)$$

For the quadratic (12), the discriminant is $\Delta = a_1^2 - 4a_0$.

When $R_e^{\text{SVIRSI}} < 1$, both $a_0 > 0$ and $a_1 > 0$. If $\Delta < 0$ the roots are complex with real part $-a_1/2 < 0$; if $\Delta \geq 0$ the roots are real with $\lambda_4 + \lambda_5 = -a_1 < 0$ and $\lambda_4\lambda_5 = a_0 > 0$, forcing both negative. Hence all eigenvalues of J_{22} have negative real parts and, together with (10), the DFE is locally asymptotically stable. Biologically, when $R_e^{\text{SVIRSI}} < 1$ each infectious host generates fewer than one secondary infection, so small perturbations decay and the infection dies out locally.

When $R_e^{\text{SVIRSI}} > 1$, then $a_0 < 0$, so $\Delta = a_1^2 - 4a_0 > a_1^2 > 0$ and $\sqrt{\Delta} > a_1$. The two roots are real and distinct,

$$\lambda_4 = \frac{-a_1 - \sqrt{\Delta}}{2} < 0, \qquad \lambda_5 = \frac{-a_1 + \sqrt{\Delta}}{2} > 0, \qquad (16)$$

so $\lambda_5 > 0$ implies instability. Biologically, a single infectious individual then produces more than one secondary infection, and the disease can invade and persist. ■

4.4.2 SIRSI Optimal Control Model

Theorem 3. The disease-free equilibrium E^0_{SIRSI} of system (2) with constant baseline controls $u_1, \ldots, u_5$ is locally asymptotically stable if $R_e^{\text{SIRSI}} < 1$, and unstable if $R_e^{\text{SIRSI}} > 1$.

Proof. At the DFE $E^0_{\text{SIRSI}} = (\Pi_h/d_1,\ 0,\ 0,\ \Pi_m/(d_2 + \Psi),\ 0)$ the Jacobian decouples exactly as in Theorem 2. The uninfected compartments contribute the negative eigenvalues $-d_1, -d_1, -(d_2 + \Psi)$, while the

© JUN 2026 | IRE Journals | Volume 9 Issue 12 | ISSN: 2456-8880
DOI: https://doi.org/10.64388/IREV9I12-1718989

infected block has characteristic equation

$\lambda^2 + a_1^{\mathrm{SIR}}\lambda + a_0^{\mathrm{SIR}} = 0$ with $a_1^{\mathrm{SIR}} = (1-u_3)\kappa + d_1 + \delta + (d_2 + \Psi) > 0$ and

$a_0^{\mathrm{SIR}} = [(1-u_3)\kappa + d_1 + \delta](d_2 + \Psi)[1 - (R_e^{\mathrm{SIRSI}})^2]$,

where R_e^{SIRSI} is the reproduction number defined in (7). The identical Routh–Hurwitz argument as in Theorem 2 then yields local asymptotic stability when $R_e^{\mathrm{SIRSI}} < 1$ (so $a_0^{\mathrm{SIR}} > 0$) and instability when $R_e^{\mathrm{SIRSI}} > 1$.

4.5 Global Stability of the Disease-Free Equilibrium

We analyse global asymptotic stability of the DFE for the two models using Lyapunov functions and LaSalle's invariance principle.

4.5.1 SVIRSI Model

For the SVIRSI model the disease-free equilibrium is

$$E_0 = (S_h^0, V_h^0, 0, 0, S_m^0, 0).$$

Theorem 4. If $R_e^{\mathrm{SVIRSI}} \le 1$, then E_0 is globally asymptotically stable in the biologically feasible region Δ.

Proof. Write the composite transmission rates $\beta_h = \zeta(1-\Theta) + (1-\mu)\alpha\lambda_h\tau_h$ and $\beta_m = \sigma\lambda_m\tau_m$; stability is governed by the same threshold R_e^{SVIRSI} defined in (5). Consider the Lyapunov function

$$L = \frac{1}{\kappa + d_1 + \delta} I_h + \frac{1}{d_2 + \Psi} I_m \ge 0. \qquad (17)$$

Differentiating along solutions and using $S_h \le S_h^0$ and $S_m \le S_m^0$, which hold in Δ,

$$\dot{L} = \left[\frac{\beta_m S_m}{d_2+\Psi} - 1\right] I_h + \left[\frac{\beta_h S_h}{\kappa + d_1 + \delta} - 1\right] I_m \le \left[\frac{\beta_m S_m^0}{d_2+\Psi} - 1\right] I_h + \left[\frac{\beta_h S_h^0}{\kappa + d_1 + \delta} - 1\right] I_m. \qquad (18)$$

When $R_e^{\mathrm{SVIRSI}} \le 1$, both bracketed coefficients are non-positive, so $\dot{L} \le 0$, with $\dot{L} = 0$ only when $I_h = I_m = 0$. The largest invariant set contained in $\{\dot{L} = 0\}$ is $\{E_0\}$, so by LaSalle's invariance principle E_0 is globally asymptotically stable.

4.5.2 SIRSI Optimal Control Model

For constant controls $u_1, \dots, u_5$, the disease-free equilibrium is $E_0 = (S_h^\circ, 0, 0, S_m^\circ, 0)$.

Theorem 5. If $R_e^{\mathrm{SIRSI}} \le 1$, then E_0 is globally asymptotically stable in the feasible region Δ.

Proof. With the Lyapunov function $L = \frac{I_h}{(1-u_3)\kappa + d_1 + \delta} + \frac{I_m}{d_2+\Psi} \ge 0$ and the transmission rates $\beta_h = (1-u_1)(1-u_2)\alpha\lambda_h\tau_h$, $\beta_m = (1-u_4)(1-u_5)\sigma\lambda_m\tau_m$, the identical computation as in Theorem 4 gives, in Δ, $\dot{L} \le [\beta_m S_m^\circ/d_2 + \Psi - 1]I_h + [\beta_h S_h^\circ/(1-u_3)\kappa + d_1 + \delta - 1]I_m$, whose bracketed coefficients are non-positive when $R_e^{\mathrm{SIRSI}} \le 1$. Hence $\dot{L} \le 0$ with equality only at $I_h = I_m = 0$, and LaSalle's invariance principle yields global asymptotic stability of E_0.

4.6 Bifurcation Analysis

We apply the Castillo-Chavez and Song centre-manifold theorem [14] to determine the type of bifurcation at $R_e = 1$ for each model. Under that

© JUN 2026 | IRE Journals | Volume 9 Issue 12 | ISSN: 2456-8880
DOI: https://doi.org/10.64388/IREV9I12-1718989

theorem, the local dynamics near $R_e = 1$ are governed by two coefficients a and b: when $a > 0$ and $b > 0$ the bifurcation is backward (subcritical), whereas when $a < 0$ and $b > 0$ it is forward (transcritical).

4.6.1 SVIRSI Model

Choose the bifurcation parameter $\varphi = (1-\mu)\alpha\lambda_h\tau_h$. At $R_e = 1$ the Jacobian has a simple zero eigenvalue, with right eigenvector w and left eigenvector v satisfying

$$w_3 > 0,\ w_6 > 0,\ w_2 < 0,\ w_5 < 0,\ w_1 < 0,\ w_4 = 0,$$
$$v_3 > 0,\ v_6 > 0,\ v_1 = v_2 = v_4 = v_5 = 0. \quad (19)$$

The non-zero second partial derivatives yield the bifurcation coefficients

$$a = v_3[2\varphi^* w_3 w_6 + 2\zeta(1-\theta)w_2 w_6] + v_6[2\sigma\lambda_m\tau_m w_3 w_5], \quad b = v_3 w_6 S_h^0. \quad (20)$$

Because the SVIRSI model includes an imperfect vaccine, a backward (subcritical) bifurcation is biologically possible, in which a stable endemic equilibrium can coexist with the DFE for R_e above a subcritical threshold $R_c < 1$. For this to occur the centre-manifold coefficient must satisfy $a > 0$ (with $b > 0$).

4.6.2 SIRSI Optimal Control Model

With bifurcation parameter $\varphi = (1-u_1)(1-u_2)\alpha\lambda_h\tau_h$, the centre-manifold computation parallels the SVIRSI case. Here the dominant right-eigenvector component $w_4 < 0$ makes the coefficient $a < 0$while $b > 0$, so the SIRSI model undergoes a forward (transcritical) bifurcation: when $R_e < 1$ only the DFE exists and is globally stable, while for $R_e > 1$ a unique stable endemic equilibrium appears. No subcritical threshold exists, so elimination is assured once $R_e$is reduced below unity.

4.7 Sensitivity Analysis

Definition 1. The normalised forward sensitivity index of R_e with respect to a parameter p, where R_e is differentiable in p, is

$$S_p^{R_e} = \frac{\partial R_e}{\partial p} \cdot \frac{p}{R_e}, \quad (21)$$

which quantifies the relative change in R_e produced by a relative change in p.

Table 5: Normalised forward sensitivity indices of R_e^{SVIRSI}.

Parameter	Index $S_p^{R_e}$	Interpretation
$\sigma,\ \lambda_m,\ \tau_m,\ \Pi_m,\ I_h$	$+0.5$	Moderate positive effect
Vaccine efficacy Θ	$-\frac{\zeta\Theta V_h^0}{2[\zeta(1-\Theta)V_h^0 + (1-\mu)\alpha\lambda_h\tau_h S_h^0]} < 0$	Negative (small) effect
Vaccination coverage μ	$-\frac{\mu}{2}\left[\frac{1}{1-\mu} + \frac{1}{\mu + d_1}\right] < 0$	Negative effect (higher coverage lowers R_e)
Mosquito natural death	$-\frac{d_2}{d_2 + \Psi}$	Negative effect

© JUN 2026 | IRE Journals | Volume 9 Issue 12 | ISSN: 2456-8880
DOI: https://doi.org/10.64388/IREV9I12-1718989

Parameter	Index $S_p^{R_e}$	Interpretation
d_2		
Vector control Ψ	$-\frac{\Psi}{d_2+\Psi}$	Negative effect
Recovery rate κ	$-\frac{\kappa}{2(\kappa+d_1+\delta)}$	Negative effect
Disease death δ	$-\frac{\delta}{2(\kappa+d_1+\delta)}$	Negative effect

Table 5 reports the elasticity of the SVIRSI reproduction number to each parameter, computed from the index (21). Because R_e^{SVIRSI} enters through a square root, the transmission-side parameters $\sigma, \lambda_m, \tau_m, \Pi_m, \Pi_h$ each carry an index of +0.5.

The transmission and recruitment parameters raise R_e, whereas vaccine efficacy Θ, enhanced mosquito mortality d_2, vector control Ψ, recovery κ, and disease-induced death δ all lower it. Vaccination coverage μ carries a negative index: higher coverage shrinks the susceptible pool and lowers R_e, as expected. The efficacy Θ also lowers R_e, though its index is small because breakthrough infection among the vaccinated (governed by the small rate ζ) contributes little to transmission.

These rankings agree with sensitivity analyses of comparable malaria-transmission models, in which vector-related transmission parameters emerge as the dominant positive drivers of R_e and vector mortality and control act as the principal negative drivers [3, 13]. The weak influence of coverage relative to efficacy is also consistent with vaccine-age-structured analyses showing that population-level impact is governed more by sustained efficacy than by coverage alone [7].

Table 6: Normalised forward sensitivity indices of R_e^{SIRSI} with respect to parameters and controls.

Parameter / Control	Index $S_p^{R_e}$	Interpretation
$\Pi_h,\ \Pi_m,\ \alpha,\ \sigma,\ \lambda_h,\ \lambda_m,\ \tau_h,\ \tau_m$	$+0.5$	Moderate positive effect
Vaccine control u_1	$-\frac{u_1}{2(1-u_1)}$	Strong negative effect
LLINs control u_2	$-\frac{u_2}{2(1-u_2)}$	Strong negative effect
Larvicide control u_4	$-\frac{u_4}{2(1-u_4)}$	Very strong negative effect
Bush clearing u_5	$-\frac{u_5}{2(1-u_5)}$	Very strong negative effect
Treatment u_3	$+\frac{\kappa u_3}{2[(1-u_3)\kappa+d_1+\delta]}$	Positive effect
Mosquito natural death d_2	$-\frac{d_2}{d_2+\Psi}$	Negative effect
Vector control Ψ	$-\frac{\Psi}{d_2+\Psi}$	Negative effect
Human death rate d_1	-1	Strong negative effect
Recovery rate κ	$-\frac{\kappa}{2[(1-u_3)\kappa+d_1+\delta]}$	Negative effect
Disease death rate δ	$-\frac{\delta}{2[(1-u_3)\kappa+d_1+\delta]}$	Negative effect

Table 6 gives the elasticity of the SIRSI reproduction number to the model parameters and to the five control efforts evaluated at the disease-free equilibrium.

© JUN 2026 | IRE Journals | Volume 9 Issue 12 | ISSN: 2456-8880
DOI: https://doi.org/10.64388/IREV9I12-1718989

The controls u_1 (vaccination), u_2 (LLINs), u_4 (larviciding), and u_5 (bush clearing) all carry strong to very strong negative indices, the larviciding and bush-clearing indices growing without bound as coverage approaches one. The treatment control u_3 shows a positive index at the DFE; in practice, however, combined with the other controls it lowers R_e. Mosquito mortality d_2, vector control Ψ, and the human death rate d_1 are negative, with d_1 the most influential, while the transmission parameters are positive at +0.5.

The prominence of integrated vector control and vaccination as negative drivers is consistent with optimal-control studies of malaria, which identify combinations of larviciding, insecticidal nets, and treatment as the most effective levers for reducing transmission [9, 20]. The positive sign of the treatment index at the DFE reflects its appearance in the recovery term of R_e rather than any harmful effect, and the practical benefit of treatment emerges once it is deployed jointly with vector control and vaccination, sustaining R_e below the elimination threshold.

V. NUMERICAL RESULTS

5.1 Numerical Simulation of the SVIRSI Model

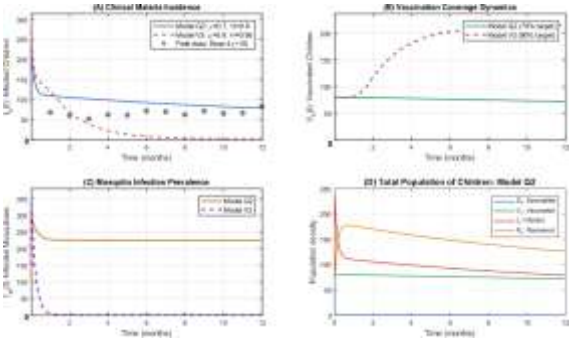

Figure 3: Numerical simulation of the SVIRSI model for MOH 710 / DHIS2 annual vaccine data, 2024, showing the effect of coverage μ and efficacy Θ.

Figure 3 shows the SVIRSI model simulated with the 2024 MOH 710 / DHIS2 annual vaccine data, with the population dynamics observed under the condition $R_e^{\text{SVIRSI}} < 1$.

Fewer children who received the vaccine became infected than in the unvaccinated comparison group, and the absolute reduction in infections increased with both vaccine coverage μ and efficacy Θ. The trajectories settle towards the disease-free state, consistent with the local and global stability results established above.

These dynamics confirm that, under $R_e < 1$, vaccinated children experience lower infection rates, with coverage and efficacy both correlating with the reduction in incidence. This is in keeping with the Phase 3 RTS,S/AS01 trial evidence and with subsequent modelling of vaccine impact in sub-Saharan Africa, which report substantial reductions in clinical malaria among vaccinated children under five [1, 4, 7].

5.2 Numerical Simulation of the SIRSI Optimal Control Model

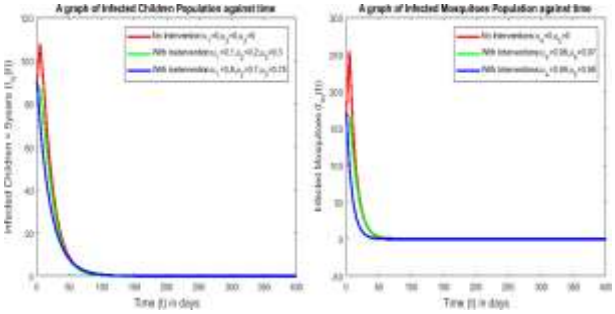

Figure 4 (left): infected children I_h; Figure 5 (right): infected mosquitoes I_m under the SIRSI optimal control model.

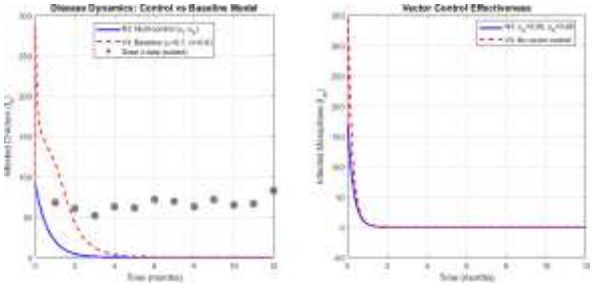

Figure 6: Numerical simulation of the SIRSI model for the 2024 vaccine data, comparing single and combined interventions.

© JUN 2026 | IRE Journals | Volume 9 Issue 12 | ISSN: 2456-8880
DOI: https://doi.org/10.64388/IREV9I12-1718989

Figures 4 and 5 present the simulated trajectories of infected children I_h and infected mosquitoes I_m with and without interventions, and Figure 6 repeats the SIRSI simulation against the 2024 data.

Vaccination u_1, in combination with LLINs u_2 and ACT treatment u_3, produces the greatest reduction in the malaria burden among children, while larviciding u_4 and bush clearing u_5 mainly reduce the infectious mosquito class. In every scenario the system converges to a stable endemic equilibrium consistent with the local data, and the joint deployment of all five interventions represents the most effective pathway towards elimination.

This complementarity between human-directed and vector-directed controls reproduces the conclusions of optimal-control analyses of malaria, which consistently identify integrated intervention packages rather than single measures as the efficient route to transmission reduction [9, 17, 20].

5.3 Malaria Vaccine Coverage Trends

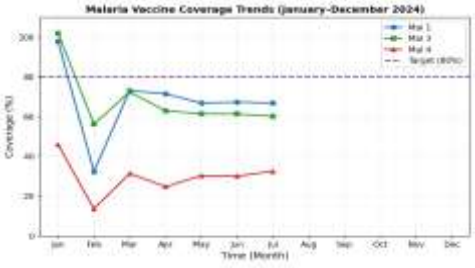

Figure 7: Malaria vaccine coverage trends (January–December 2024) for Mal 1, Mal 3, and Mal 4 against the 80% target.

Figure 7 visualises the monthly Mal 1, Mal 3, and Mal 4 coverage from Table 2 against the 80% target, making plain the collapse of the Mal 4 booster (29.3%) relative to the near-target first-three-dose coverage; the programmatic implications and supporting literature are discussed under Table 2.

5.4 Cost-Effectiveness Analysis

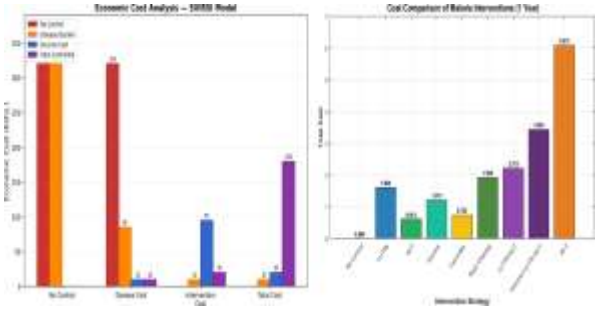

Figure 8 (left): economic cost analysis (SVIRSI model), a 43.75% total-cost reduction through vaccination; Figure 9 (right): cost comparison of intervention strategies for the SIRSI model.

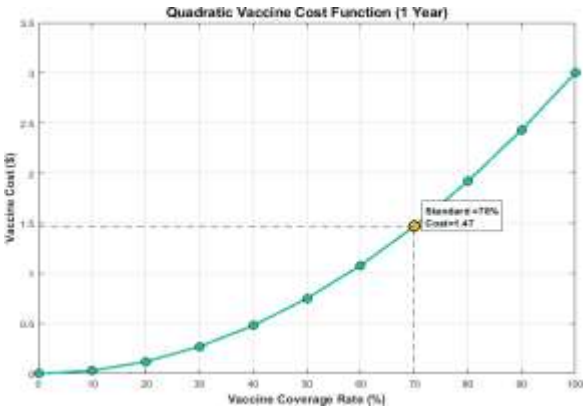

Figure 10: Cost-effectiveness plane relating vaccine cost and coverage.

Figures 8 to 10 summarise the economic evaluation: Figure 8 shows that, under the SVIRSI model, vaccine intervention yields a 43.75% reduction in total economic cost; Figure 9 compares the cost of the different intervention strategies for the SIRSI model; and Figure 10 displays the cost-effectiveness plane relating vaccine cost to coverage.

The combination of vaccination, LLINs, and ACT treatment gives the lowest incremental cost-effectiveness ratio (ICER) per additional infection averted, making it the most economically efficient strategy, while the full five-intervention package averts the most infections at a higher incremental cost.

This accords with the broader evidence that malaria vaccination is cost-effective by standard measures when delivered alongside existing control tools [4,

11, 24]. Taken together with the simulation and coverage results, the analysis provides quantitative validation, calibrated to local data, for malaria control in Bungoma County.

VI. CONCLUSION AND RECOMMENDATIONS

The WHO-recommended schedule of a first dose at six months with a booster at 18 months is supported by the model's qualitative results for Bungoma County, and the RTS,S/AS01 vaccine is projected to substantially reduce malaria incidence in children under five. However, current booster (Mal 4) coverage is severely inadequate at 29.3% with a 47.2% dropout rate, requiring urgent programmatic action.

On this basis we recommend administering the first dose at six months and the booster at 18 months as validated by the model; strengthening follow-up and defaulter tracing for the booster dose to reduce dropout; and implementing the most cost-effective strategy, which combines vaccination with long-lasting insecticidal nets and artemisinin-based combination therapy, while integrating vaccination with existing mosquito-control measures.

VII. ACKNOWLEDGEMENT

The authors gratefully acknowledge the Department of Mathematics, Kibabii University, for providing the academic environment and institutional resources that supported this research. We thank the Health Director of Bungoma County Referral Hospital and Dr. David Ikura Shivachi, Medical Officer of Health at Bumula Sub-County Hospital, for authorising access to the secondary malaria vaccine data essential for model parameterisation and validation. We are grateful to Dr. Wachira Charles of the Department of Mathematics, Machakos University, for scholarly discussions that strengthened the mathematical analysis, and to Mr. Ronald Kiplangat, Public Health Officer at Sirisia Sub-County Hospital, for clinical input on local malaria control and vaccine implementation.

REFERENCES

[1] Olotu A, Leach A. Efficacy of RTS,S/AS01 malaria vaccine administered according to different schedules in African children: a randomised trial. Lancet. 2016;387(10016):367–375. doi:10.1016/S0140-6736(14)01023-5

[2] Chataa P, Gideon KG. Analysis of a malaria transmission model with vaccination proportion and vaccine-induced immunity. Math Comput Appl. 2025;30(1):15. doi:10.3390/mca30010015

[3] Griffin JT, Lynch M. Potential for reduction of burden and local elimination of malaria by reducing Plasmodium falciparum malaria transmission: a mathematical modelling study. Lancet Infect Dis. 2016;16(4):465–472. doi:10.1016/S1473-3099(14)00423-5

[4] Hogan AB, Winskill P. Estimated impact of RTS,S/AS01 malaria vaccine allocation strategies in sub-Saharan Africa: a modelling study. PLoS Med. 2020;17(11):e1003377. doi:10.1371/journal.pmed.1003377

[5] Opicho DS, Kwach B, Nyukuri R. A mathematical model for malaria transmission dynamics with vaccination as a control variable in children under five years of age. IRE Journals. 2026;9(11). doi:10.64388/IREV9111-1718271

[6] Thomann L, Hérau F. On global existence and trend to the equilibrium for the Vlasov–Poisson–Fokker–Planck system with exterior confining potential. J Funct Anal. 2016; 271:1301–1340. doi: 10.1016/j.jfa.2016.05.012

[7] Vogt-Geisse K, Feng Z. The impact of vaccination on malaria prevalence: a vaccine-age-structured modeling approach. J Biol Syst. 2020;28(2):475–513. doi:10.1142/S0218339020400091

[8] Muller GE, Vyambwera M, et al. Stability and control in a stochastic model of malaria population dynamics. Adv Contin Discrete Models. 2023. doi:10.1186/s13662-023-03791-3

[9] Mwamtobe PMM. Optimal control of intervention strategies for malaria epidemic in Karonga District, Malawi. PhD thesis. University of the Witwatersrand; 2014.

[10] Ototo EN, Kamau L. Age-specific Plasmodium parasite profile in pre and post ITN intervention period at a highland site in western Kenya. Malar J. 2017;16:466. doi:10.1186/s12936-017-2116-5

[11] Penny MA, Camponovo F, Chitnis N, Smith TA, Tanner M. Future use-cases of vaccines in malaria control and elimination. Parasite Epidemiol Control. 2020;10:e00145. doi:10.1016/j.parepi.2020.e00145

[12] World Health Organization. Malaria profile and socio-economic predictors among under-five children: analysis of 11 sub-Saharan African countries. Malar J. 2023;22:55. doi:10.1186/s12936-023-04478-6

[13] van den Driessche P, Watmough J. Reproduction numbers and sub-threshold endemic equilibria for compartmental models of disease transmission. Math Biosci. 2002;180:29–48.

[14] Castillo-Chavez C, Song B. Dynamical models of tuberculosis and their applications. Math Biosci Eng. 2004;1(2):361–404.

[15] Bangirana P, Ssenyonga P. Long-term effects of severe malaria and its treatment on cognition and behaviour among Ugandan children. J Neuroparasitol. 2022;13. doi:10.1186/s13071-022-05386-6

[16] Ezekiel C, Alice L. Predictors of malaria vaccine hesitancy among caregivers in Bumula Sub-County, Bungoma County. Pediatr Res. 2023;13(1):15–31.

[17] Okosun O, Kazeem O, et al. Global stability and optimal control analysis of malaria dynamics in the presence of human travelers. Ladoke Akintola University of Technology, Nigeria; 2018.

[18] Greenwood B, Dicko A. Malaria vaccine development: progress and challenges. Nat Rev Immunol. 2022;22(7):418–430.

[19] Castro MC, Chiyaka C, et al. Malaria incidence rates from time series of 2-wave panel surveys. PLoS Comput Biol. 2016;12(8):e1005065.

[20] Gabriel O, Joseph K, et al. Transmission dynamics and optimal control of malaria in Kenya. Discrete Dyn Nat Soc. 2016;8013574.

[21] Baghani H, Ramezani M. Orthogonal sets: their relation to the axiom of choice and a generalized fixed point theorem. J Fixed Point Theory Appl. 2016;18(3):465–477.

[22] Moturi AK, Jalang'o R, Cherono A, Muchiri SK, Snow RW, Okiro EA. Malaria vaccine coverage estimation using age-eligible populations and service user denominators in Kenya. Malar J. 2023;22(1):287. doi:10.1186/s12936-023-04721-0

[23] Okyere J, Bediako VB, Ackah JA, et al. RTS,S/AS01E vaccine defaults in Ghana: a qualitative exploration of the perspectives of defaulters and frontline health service providers. Malar J. 2023;22(1):260. doi:10.1186/s12936-023-04690-4

[24] World Health Organization. Malaria vaccines (RTS,S and R21): questions and answers. Geneva: WHO; 2024.